ARTICLE

Whispering Gallery Mode Lasing from Zinc Oxide Hexagonal Nanodisks

Daniel J. Gargas,[†] Michael C. Moore,[†] Adrian Ni,[‡] Shu-Wei Chang,[‡] Zhaoyu Zhang,[†] Shun-Lien Chuang,[‡] and Peidong Yang[†,*]

[†]Department of Chemistry, University of California, Berkeley, California 94720, and Materials Sciences Division, Lawrence Berkeley National Laboratory, 1 Cyclotron Road, Berkeley, California 94720 and [‡]Department of Electrical and Computer Engineering, University of Illinois at Urbana–Champaign, Urbana, Illinois 61801

ABSTRACT Disk-shaped semiconductor nanostructures provide enhanced architectures for low-threshold whispering gallery mode (WGM) lasing with the potential for on-chip nanophotonic integration. Unlike cavities that lase *via* Fabry—Perot modes, WGM structures utilize low-loss, total internal reflection of the optical mode along the circumference of the structure, which effectively reduces the volume of gain material required for lasing. As a result, circularly resonant cavities provide much higher quality (*Q*) factors than lower reflection linear cavities, which makes nanodisks an ideal platform to investigate lasing nanostructures smaller than the free-space wavelength of light (*i.e.*, subwavelength laser). Here we report the bottom-up synthesis and single-mode lasing properties of individual ZnO disks with diameters from 280 to 900 nm and show finite difference time domain (FDTD) simulations of the whispering gallery mode inside subwavelength diameter disks. These results demonstrate ultraviolet WGM lasing in chemically synthesized, isolated nanostructures with subwavelength diameters.

KEYWORDS: ZnO · lasing · whispering gallery · disk · mode simulation

WGM lasing has been demonstrated in a variety of materials and circular structures.[1−10] Recent studies have shown ultra-low-threshold continuous-wave lasing microdisks,[11] high-Q silicon nanocrystal resonators,[12,13] and visible and near-IR lasing in subwavelength diameter structures.[14,15] Although there has been much progress on nanoscale WGM lasers, most reports utilize top-down fabricated materials such as quantum wells or embedded quantum dot layers that require numerous fabrication steps as well as subsequent patterning.

Bottom-up synthesized nanostructures, on the other hand, have inherent advantages over top-down fabricated structures such as high crystallinity, smooth surface faceting, material homogeneity, sample density, and high-throughput assembly. Several reports have shown nanowire and nanorod lasers grown on various substrates, in both high-density and dilute arrays.[16−20] However, for WGM structures that require low aspect ratios, there exist significant challenges in realizing bottom-up grown WGM lasers with nanoscale dimensions. An additional challenge concerning WGM structures is that the optical gain in a nanoscale resonator must be sufficiently high to compensate for low optical mode confinement. As the diameter is reduced, the WG mode extends further out of the disk, which results in less perfect mode overlap with the gain material. Therefore, to maximize optical gain and minimize nonradiative processes, nanodisks with high crystallinity and low defect density are essential. Finally, spatial isolation is also crucial for optically investigating single nanoscale lasers, which, depending on the method of optical pumping, requires approximately 2−10 μm between nanodisks. Up to this point, reports on bottom-up synthesized nanodisks have not stressed optical isolation for individual optical characterization.

To investigate subwavelength nanodisk lasing, ZnO was chosen due to its high exciton binding energy, high optical gain, and propensity for room temperature UV lasing. Single-step methods for growing highly crystalline ZnO nanostructures have been well-studied, and a variety of shapes have been demonstrated. ZnO growth by chemical vapor transport (CVT), for example, yields faceted structures such as microwires,[21] microdisks,[22] and nanonails,[23,24] and optimization of experimental conditions can yield moderate control over the structure diameter. To date, the smallest diameter of the ZnO structures reported in WGM lasing is 650 nm.[24] However, in most reports, it is not clear as to which structure was optically characterized. Moreover, since the band edge PL is approximately 385 nm, WGM lasing has yet to be observed in subwavelength ZnO structures. Lastly, recent synthetic methods have shown dilute

*Address correspondence to p_yang@berkeley.edu.

Received for review December 12, 2009 and accepted April 20, 2010.

Published online April 23, 2010. 10.1021/nn9018174

growth of ZnO nanostructures with sufficiently low density for isolated optical characterization.[17] Building on these efforts, we report lasing characterization on individual ZnO nanodisks, with corresponding dimensional analysis by electron microscopy, to investigate the nature of WGM lasing in subwavelength structures.

RESULTS AND DISCUSSION

A modified CVT process was utilized for bottom-up synthesis of faceted ZnO nanodisks. The synthesis procedure is an adaptation of ZnO tetrapod growth using a chemical vapor transport and condensation method,[25] in which straight wall structures were formed at low oxygen concentration (0.5−5%), whereas the tapered walls were formed at high oxygen concentration (5−10%). For our studies, the reaction temperature was set to 800−900 °C and the reaction time was approximately 15 min (after a 12 min temperature ramp period) with an oxygen concentration of 0.5%. The low oxygen concentration resulted in growth of low-density arrays of ZnO cylinders and rods. Decreasing the reaction time to 0−3 min (after a 12 min ramp period) resulted in smaller structures with lower aspect ratios. To reduce the dimensions of ZnO nanodisks even further, the reaction temperature was lowered to 700−750 °C and run for 0−5 min. In addition to the size reduction, the lower temperature and shorter reaction times resulted in the formation of ZnO nanodisks with tapered bases.

With regard to the formation of tapered-base structures at low reaction temperature, it is suspected that the relationship between morphology and oxygen concentration depends mainly on the ratio of oxygen to zinc partial pressures. For the synthesis used in this study, the decreased reaction temperature resulted in a significantly lower Zn partial pressure, whereas the oxygen partial pressure was kept constant. While the mechanism behind the formation of tapered nanodisks is not exactly understood, our results agree with the previous report that growth of different ZnO crystal faces is kinetically controlled by the partial pressure of the reactants. Most importantly, low-density growth was achieved on silica substrates by limiting reagent concentrations, which resulted in dilute arrays with distances approximately 5−10 μm between neighboring disks. This leads to high-quality ZnO nanodisks that were isolated for individual optical and electron microscope characterization without additional steps of post-growth transfer.

An illustration depicting the lasing of a whispering gallery mode is shown in Figure 1a, in which an optical mode internally reflects off the side walls of a hexagonal disk and escapes into the far-field. As opposed to Fabry−Perot modes, which achieve lasing by reflecting off the end facets of a linear cavity, whispering gallery modes undergo total internal reflection around the walls of the disk. At a reflection angle of 30°, over 96% of the optical mode is reflected at the ZnO−air interface, thus whispering gallery modes provide low-loss, high-efficiency resonant pathways for optical gain. Eventually, whispering gallery lasing modes leak into the plane or scatter in the vertical direction *via* surface irregularities.

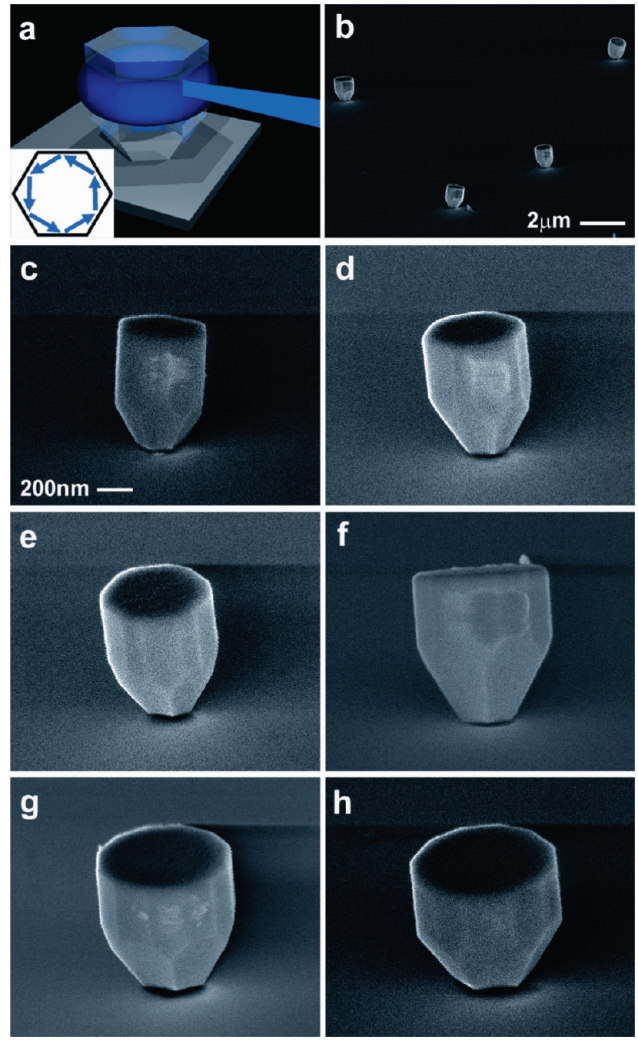

Figure 1. Whispering gallery mode lasing in ZnO nanodisks. (a) Nanodisk illustration showing whispering gallery mode coupling into the plane or vertical direction *via* surface scattering, (b) far-field SEM image of ZnO nanodisks grown by CVT on a SiO_2 substrate, and (c−h) SEM images of various diameter ZnO nanodisks with hexagonal or truncated hexagonal faceting, which supports whispering gallery mode lasing. Disk diameters (measured edge to edge) are (c) 491 nm, (d) 561 nm, (e) 612 nm, (f) 750 nm, (g) 785 nm, and (h) 815 nm.

Figure 1b shows spatially isolated ZnO nanodisks grown on a silica substrate. Low-density arrays ideal for individual optical characterization were achieved by optimizing oxygen concentration and reaction temperature during synthesis. Figure 1c−h shows cross-section scanning electron microscopy (SEM) images of CVT grown ZnO nanodisks with diameters varying from 491 to 815 nm. Diameters were measured from edge to edge. However, as optical simulations will show, the WG mode is in close proximity to the sharp corners,

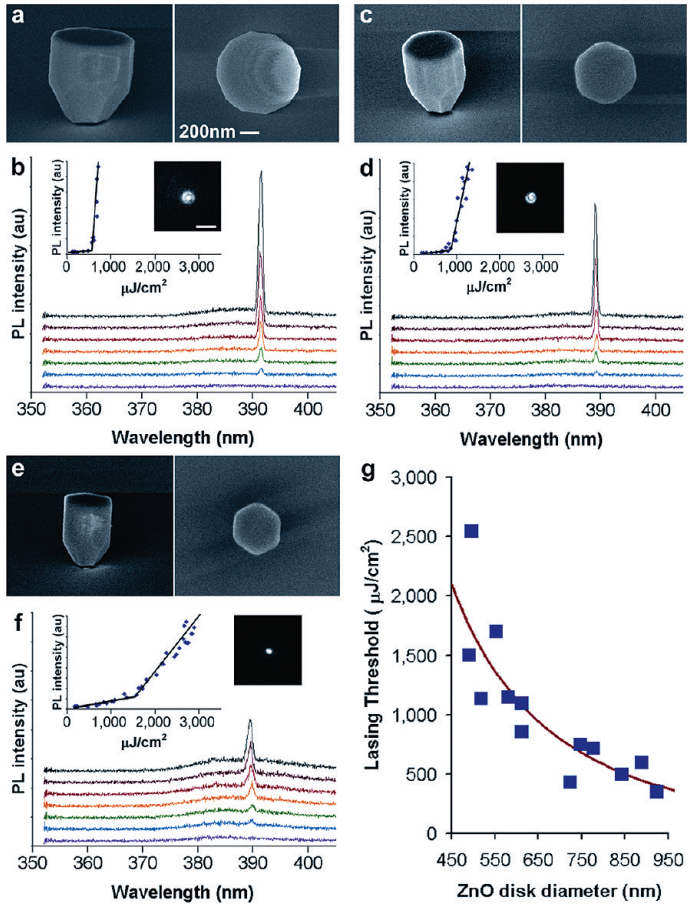

Figure 2. Room temperature, single-mode lasing properties of ZnO nanodisks with various diameters. Cross-section and top-down SEM images of ZnO nanodisks are shown with diameters of (a) 842 nm, (c) 612 nm, and (e) 491 nm. Lasing spectra collected at increasing pump powers are shown in (b), (d), and (f) for corresponding nanodisks in (a), (c), and (e). Inset graphs show integrated PL intensity *vs* pump power, and PL images of nanodisk lasing (scale bar =10 μm). (g) Room temperature lasing threshold *vs* disk diameter. ZnO nanodisk lasing thresholds (blue squares) are plotted as a function of nanodisk diameter. The curve (red line) is the best fit to a $1/D^2$ trend.

thus hexagonal disks must overcome greater mode loss than those of top-down fabricated circular disks.

Interestingly, the base of each ZnO nanodisk is tapered such that the region in contact with the substrate is significantly smaller than the nanodisk diameter. This reduces the area of low-contrast index at the ZnO−silica interface, which normally couples the optical mode into the substrate and hinders the lasing process. Instead, the tapered base provides a high index contrast barrier and acts as a reflector. In effect, it pushes the optical mode away from the substrate and confines it more to the upper part of the nanodisk. This process optimizes mode overlap with the ZnO gain medium, and more efficient lasing is achieved. Unlike top-down fabricated disks, the tapering process for ZnO nanodisks occurs naturally during CVT growth, which eliminates the need for additional steps to isolate the optical mode within the disk, such as back-etching or substrate removal.

Figure 2 shows photoluminescence (PL) spectra from various ZnO nanodisks with different diameters when optically pumped by pulsed laser at room temperature (see Methods). The large nanodisk in Figure 2a has a diameter of 842 nm and a height of 750 nm and reveals a tapered base approximately 300 nm high. At low pump powers, the PL spectrum is broad and featureless (Figure 2b, bottom curve); however, as the pump power is increased above the lasing threshold, a lasing peak appears at 391 nm with a full width at half-maximum (fwhm) line width of 0.8 nm. A plot of the integrated peak intensity *versus* pump power (Figure 2b, inset) shows a sharp rise at approximately 500 μJ/cm^2, which indicates the transition from spontaneous to stimulated emission.[26] A log−log plot of the integrated peak intensity is shown in Figure S1 (Supporting Information). Figure 2c shows a medium sized nanodisk with a diameter of 612 nm and a height of 550 nm, also with a tapered base. Similar to the larger disk, a lasing peak at 389 nm with a fwhm line width of 0.7 nm appears as the pump power is increased above the lasing threshold (Figure 2d). While one would expect the lasing peak to blue shift as the disk diameter is reduced, in reality, the lasing wavelength is determined by the overlap of the WG mode within the gain medium spectral bandwidth of ZnO (*i.e.*, the peak modal gain), which for most disks occurred between 385 and 391 nm. As observed in Figure 2, a reduction in disk diameter causes the lasing mode to shift into the spectral window of optimal gain at approximately 390 nm. While the nanodisks shown in Figure 2 exhibit single-mode lasing, multiple lasing modes were observed for disks with diameters of approximately 1 μm and larger (Figure S2, Supporting Information).

The power dependence plot for the 612 nm disk (Figure 2d, inset) shows a slightly larger lasing threshold of 860 μJ/cm^2. The increase in lasing threshold can be attributed to the smaller nanodisk cavity volume. A smaller diameter provides less spatial overlap between the WG mode and the ZnO gain medium, resulting in an optical mode that "spills" out of the external boundary of the nanodisk.[4] This reduced confinement causes a decrease in quality factor (Q) due to the increase of the leakage power. This effect is even more pronounced in the smaller nanodisk shown in Figure 2e, which has a diameter of 491 nm and a lasing threshold of 1500 μJ/cm^2 (Figure 2f, inset). The lasing spectra in Figure 2f show a slower onset of the lasing peak at 390 nm and a larger fwhm of 1.2 nm, which indicates a more lossy nanodisk cavity and lower quality lasing mode.

A plot of ZnO nanodisk diameter *versus* lasing threshold at room temperature is shown in Figure 2g. The best-fit line (red curve) is approximately $1/D^2$, which suggests the lasing threshold is dependent on multiple parameters involving nanodisk diameter. Previous studies show both WG mode quality factor (Q) and confinement factor (Γ) depend on disk diameter,[3,27] and

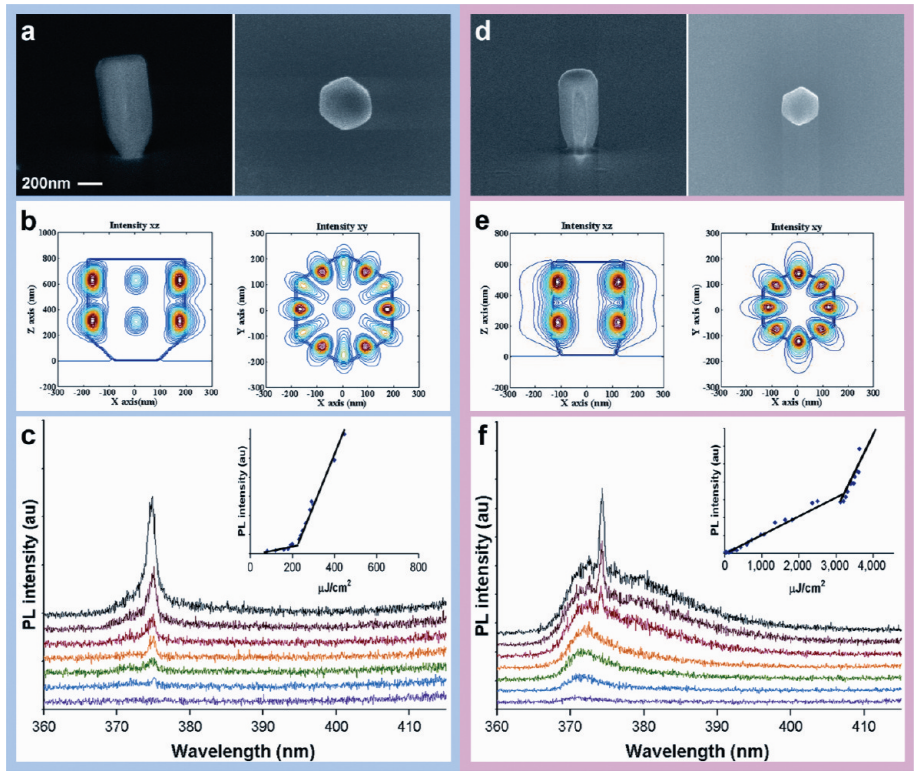

Figure 3. Lasing properties of subwavelength ZnO nanodisks at 8 K. Cross-section and top-down SEM images showing nanodisks with dimensions (height × diameter) of (a) 791 nm × 375 nm and (d) 606 nm × 283 nm. Optical mode simulations of the calculated $|E|^2$ field in the *xy* plane are shown in (b) and (e) for nanodisks in (a) and (d), respectively. Lasing spectra at increasing pump energies are shown in (c) and (f) for nanodisks in (a) and (d), respectively. Inset graphs show integrated PL intensity *vs* pump power.

since lasing threshold is inversely proportional to Q and Γ, a $1/D^2$ relationship is expected for disk diameter and lasing threshold. Most importantly, the lasing threshold scales inversely with the power of nanodisk diameter, rather than disk height, which is evidence of whispering gallery mode lasing rather than Fabry−Perot lasing in the vertical direction.

Due to the reduction in optical mode confinement with decreasing nanodisk size, at a certain diameter, the cavity losses outweigh the optical gain and lasing will not occur. Utilizing our control of nanodisk diameter, we set out to determine the smallest diameter ZnO disk that can achieve lasing. For room temperature lasing, this occurs at approximately 490 nm. However, to achieve whispering gallery mode lasing in a subwavelength diameter disk, we optically pumped nanodisks at a temperature of 8 K. Low temperature facilitates the lasing process in ZnO nanodisks in two ways: (1) nonradiative processes associated with phonon coupling are significantly reduced; and (2) high-intensity excitation can be probed without causing thermal damage to the nanodisks. Figure 3 shows two subwavelength diameter disks that achieved lasing at 8 K. SEM images of the nanodisks with dimensions (height × diameter) of 791 nm × 375 nm and 606 nm × 283 nm are shown in Figures 3a,b, respectively. The 375 nm diameter disk exhibits a clear lasing peak at approximately 375 nm and a lasing threshold at roughly 250 μJ/cm^2 (inset). Similarly, the 283 nm diameter disk shows a lasing peak at approximately 374 nm, however, at a much larger threshold of 3000 μJ/cm^2. As discussed above, the increased lasing threshold is due to the reduced diameter, particularly when it is smaller than the free space lasing wavelength. Especially in the case of the 283 nm diameter disk, significant portion of the whispering gallery mode exists outside the nanodisk, which results in much less overlap with the ZnO gain medium.

To quantify the overlap between the whispering gallery mode and the ZnO nanodisk, optical mode simulations were performed by finite difference time domain (FDTD) method,[28] using a freely available software package with subpixel smoothing for increased accuracy.[29] FDTD simulations were used instead of a conventional method based on effective optical path length (ray optics) due to the small diameter of the nanodisks. For larger cavities, one can usually estimate the threshold gain of the fundamental whispering gallery mode using the effective optical path length around the cavity, which is proportional to the edge length of the polygon.[3,4] Specifically, this type of the estimation is based on the analogue of traveling wave lasers, in which the wave amplitude has to return to itself after absorption/amplification during the wave propagation, and transmission loss occurs whenever the fictitious ray of the lasing mode hits the polygon surface. It should be noted that the validity of this ap-

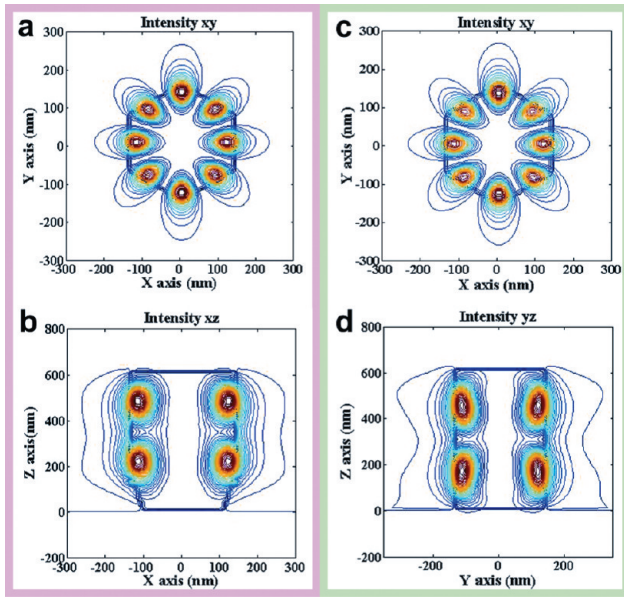

Figure 4. Whispering gallery optical mode simulations of a subwavelength ZnO nanodisk with and without a tapered base. Calculated $|E|^2$ field of the nanodisk with dimensions of 283 nm × 606 nm (diameter × height) in the (a) *xy* plane and (b) *yz* plane. The calculated mode has a resonant wavelength of 374 nm and a quality factor of 93. The simulations shown in (c) and (d) are for the same nanodisk without the tapered base. This mode has similar field patterns in the *xy* and *yz* planes to those in (a) and (b) except for the field above the substrate surface. Its wavelength and *Q* are 378 nm and 77, respectively. Comparing (b) and (d), the tapered-base nanodisk has less field penetrating into the substrate, leading to a higher quality factor.

proximation lies in the well-guided modal profile along the growth direction of the polygon cavity and assumes the diameter of the disk is much larger than the resonant wavelength, namely, the radiation loss is dominated by the power leakage at the side walls, not from the top and bottom of the polygon. However, with the decrease of the disk diameter close to the resonant wavelength, more field penetrates into the substrate below or leaks out the disk from the top. From the FDTD calculations, although the main radiation losses indeed come from the side walls, those from the top and bottom of the nanodisk are not negligible. Furthermore, the field profile from the FDTD calculation indicates that the possible lasing modes are not fundamental whispering gallery mode of the polygon cavity. These facts make the estimation of the threshold gain of this 3D polygon cavity from an *effective optical length* impractical.

Instead, the proper way to estimate the threshold gain, G_{th}, of a possible lasing mode is to use the formula below:

$$G_{th} = \frac{2\pi n_g}{\Gamma_E \lambda Q} \quad (1)$$

where n_g, λ, Γ_E, and Q are group index of the material, resonant wavelength, energy confinement factor, and quality factor, respectively. This relation originates from the general gain−loss balance condition of the rate equation and is valid for all types of cavity modes. In our case, the FDTD calculation can give λ, Γ_E, and Q. Since in the calculation the material loss is assumed to be small, the calculated quality factors in the paper are from the radiation losses of the cavity, which include power leakages in *all directions*. Accordingly, G_{th} values for different structures can be obtained. Detailed derivations of this formula are shown in ref 30.

Using this method, $|E|^2$ field intensities were calculated for the horizontal and vertical planes of the 375 and 283 nm diameter disks and are shown in Figure 3b and 3e, respectively. The calculated mode wavelengths for the 375 and 283 nm diameter disks are 376 and 374 nm, respectively, which agree well with the experimentally observed lasing peaks. For the 283 nm diameter disk, the optical energy confinement factors[30] of the polarization components parallel ($\Gamma_\parallel$) and normal ($\Gamma_\perp$) to the silica substrate are 0.105 and 0.541, respectively, and the quality factor (Q) is 93. Despite having a diameter much less than the wavelength of the lasing mode, the 283 nm disk managed to contain almost 65% of the mode energy within its structure. This is, in part, due to the tapered base that pushes the mode away from the substrate into the upper part of the nanodisk.

To quantitatively compare the advantages of a tapered-base cavity, the energy confinement factor and Q were also calculated for a 283 nm diameter cavity with vertical side walls. A comparison of the nanodisk mode patterns with and without a tapered base is shown in Figure 4. In the nontapered structure, the optical energy confinement factors, $\Gamma_\parallel$ and $\Gamma_\perp$, of the nanodisk are 0.092 and 0.521, respectively, and Q is only 77. Consequently, more field penetrates into the substrate, which indicates that the tapered-base geometry confines the mode in the nanodisk better. This results in the smaller leakage power from the substrate. For a nanodisk with a tapered base, the quality factor is improved by 20.7%, and the corresponding threshold material gain can be decreased from 10 889 to 7351 cm^{-1}.

To further investigate the effect of the tapered-based structure on the leakage power, we calculate the ratio of the leakage power from the substrate over the total leakage power and compare these values for tapered-based and vertical side wall structures. The leakage power is calculated by simulating an artificial box that encompasses the nanodisk as well as a portion of the substrate underneath. The Poynting vectors are then determined by the FDTD program, which yields the corresponding radiation powers from the six facets of the box at any moment. To obtain the radia-

TABLE 1. Leakage Power Ratio

	leak power ratio		
	side wall	air	substrate
tapered base	0.738	0.090	0.172
vertical side walls	0.723	0.091	0.186

tion powers of a specific resonant mode, the mode is excited using a dipole source with a narrow bandwidth. After the source is turned off, the radiation powers from all six facets are calculated in time. To obtain the averaged radiation power, the radiation powers are summed over several optical cycles and divided by the total optical cycles.

This method is used to calculate the leakage powers from the top (P_{air}), side walls (P_{xy}), and bottom (P_{sub}) of the simulated box for the structures with and without tapered bases. The ratios for each component over the total leakage power, the sum of P_{air}, P_{xy}, and P_{sub}, for both cases are tabulated in Table 1.

The ratios of P_{sub} over the total leakage power for tapered base and vertical side wall cases are 0.172 and 0.186, respectively. The calculation shows that the radiation power from the substrate can be reduced by 7.5% using the tapered base. Although the energy confinement factors Γ_E in the nanodisk for these two cases are only 3% different, the confinement factors in the substrate are 0.168 in the tapered-base case and 0.213 in the vertical side wall case. This indeed shows that more energy leaks into the substrate for the vertical side wall case.

By combining a low-loss lasing mechanism into a high-gain semiconductor material, ZnO nanodisks have achieved lasing in the smallest diameter WGM structures to date. The observed lasing in 491 and 283 nm diameter disks at room temperature and low temperature (8 K), respectively, represents the smallest diameter semiconductor structures for both chemically synthesized and top-down fabricated WGM structures. Furthermore, when normalized to the refractive index at the lasing wavelength (ZnO = 2.45, GaAs = 3.5, InP = 3.5), ZnO nanodisks exhibit the lowest ratios of diameter-to-lasing wavelength that were previously demonstrated with InGaAs and InP WGM disks at near-IR wavelengths.[14,15]

CONCLUSION

In summary, we have demonstrated a bottom-up synthesis of ZnO nanodisks with diameters from 280 to 900 nm that are spatially isolated for individual optical characterization. Room temperature, ultraviolet lasing was observed in nanodisks as small as 491 nm in diameter, and an inverse trend in lasing threshold with disk diameter is observed. At low temperatures, lasing was observed in a subwavelength diameter disk (283 nm), which is the smallest diameter WGM lasing structure reported to date. In addition, FDTD simulations show a 7.5% reduction in radiative power lost to the substrate, as well as a 20.7% increase in *Q* factor, for nanodisks with a tapered-base structure. These findings open up promising avenues for mass-scale production of nanoscale lasers and on-chip devices for nanophotonics.

METHODS

ZnO hexagonal nanodisks were synthesized by a home-built chemical vapor transport system. Zn powder (Alfa Aesar, 99.999%) was used as Zn source. The source material was placed in an alumina boat located in the center of a quartz tube in a tube furnace. Ultrasonically cleaned silicon oxide substrates (600 nm thermal oxide layer) were placed 3 cm downstream of the carrier gas flow. A mixture of 0.5−1.5% O_2 in Ar was used as the carrier gas with a flow rate of 10−12 sccm. The reaction chamber was purged using carrier gas before starting the reaction. The reaction temperature was set to 800−900 °C, and the reaction time was approximately 15 min (after a 12 min temperature ramp period) with an oxygen concentration of 0.5%. The low oxygen concentration resulted in growth of low-density arrays of ZnO cylinders and rods. Decreasing the reaction time to 0−3 min (after a 12 min ramp period) resulted in smaller structures with lower aspect ratios. To reduce the dimensions of ZnO nanodisks even further, the reaction temperature was lowered to 700−750 °C and run for 0−5 min. Scanning electron microscopy was performed on a JEOL JSM-6340F field-emission SEM operating at 5 kV.

PL measurements on individual ZnO nanodisks were performed using 266 nm excitation from a Q-switched Nd:YAG laser (Spectra-Physics, 8 ns pulse, 10 Hz, 1−100 μJ/pulse) focused to a beamspot approximately 10 μm in diameter at a grazing angle ~70° normal to the substrate. The sample was placed on an *X*−*Y*−*Z* translation stage of a dark-field microscope, whereby PL emission was collected with a 50× objective (0.5 NA) and routed to an EMCCD camera for imaging (Andor) or to a LN-cooled CCD/spectrometer (PI Acton) *via* optical fiber. The spectral resolution of the instrument is 0.05 nm using a 1200 grooves/mm grating. PL spectra were averaged over 100 pulses to minimize pulse energy deviation. Power dependence curves were calculated from the integrated PL signal of the lasing mode plotted *versus* incident pulse energy density. Where specified, low-temperature studies were performed with a liquid helium cryostat (Janus).

Acknowledgment. This work was supported by the DARPA NACHOS program. P.Y. would like to thank NSF for the A.T. Waterman Award. The authors thank Ruoxue Yan for assistance with figure illustration.

Supporting Information Available: Power dependence data of ZnO nanodisk lasing plotted on a log−log scale and multimode lasing observed in large diameter disks. This material is available free of charge *via* the Internet at http://pubs.acs.org.

REFERENCES AND NOTES

1. McCall, S. L.; Levi, A. F. J.; Slusher, R. E.; Pearton, S. J.; Logan, R. A. Whispering-Gallery Mode Microdisk Lasers. *Appl. Phys. Lett.* **1992**, *60*, 289–291.
2. Michler, P.; Kiraz, A.; Becher, C.; Schoenfeld, W. V.; Petroff, P. M.; Zhang, L. D.; Hu, E.; Imamoglu, A. A Quantum Dot Single-Photon Turnstile Device. *Science* **2000**, *290*, 2282–2285.
3. Bhowmik, A. K. Polygonal Optical Cavities. *Appl. Opt.* **2000**, *39*, 3071–3075.
4. Wiersig, J. Hexagonal Dielectric Resonators and Microcrystal Lasers. *Phys. Rev. A* **2003**, *67*, 023807.
5. Vahala, K. J. Optical Microcavities. *Nature* **2003**, *424*, 839–846.
6. Hovinen, M.; Ding, J.; Nurmikko, A. V.; Grillo, D. C.; Han, J.; He, L.; Gunshor, R. L. Blue-Green Laser-Emission from ZnSe Quantum-Well Microresonators. *Appl. Phys. Lett.* **1993**, *63*, 3128–3130.

7. Mahler, L.; Tredicucci, A.; Beltram, F.; Walther, C.; Faist, J.; Witzigmann, B.; Beere, H. E.; Ritchie, D. A. Vertically Emitting Microdisk Lasers. *Nat. Photonics* **2009**, *3*, 46–49.
8. Min, B. K.; Ostby, E.; Sorger, V.; Ulin-Avila, E.; Yang, L.; Zhang, X.; Vahala, K. High-Q Surface-Plasmon-Polariton Whispering-Gallery Microcavity. *Nature* **2009**, *457*, 455–458.
9. Srinivasan, K.; Painter, O. Linear and Nonlinear Optical Spectroscopy of a Strongly Coupled Microdisk-Quantum Dot System. *Nature* **2007**, *450*, 862–865.
10. Wiersig, J.; Gies, C.; Janke, F.; Abmann, M.; Berstermann, T.; Bayer, M.; Kistner, C.; Reitzenstein, S.; Schneider, C.; Hofling, S.; Frochel, A.; Kalden, J.; Hommel, D. Direct Observation of Correlations between Individual Photon Emission Events of a Microcavity Laser. *Nature* **2009**, *460*, 245–250.
11. Tamboli, A. C.; Haberer, E. D.; Sharma, R.; Lee, K. H.; Nakamura, S.; Hu, E. L. Room-Temperature Continuous-Wave Lasing in GaN/InGaN Microdisks. *Nat. Photonics* **2007**, *1*, 61–64.
12. Ghulinyan, M.; Navarro-Urrios, D.; Pitanti, A.; Lui, A.; Pucker, G.; Pavesi, L. Whispering-Gallery Modes and Light Emission from a Si-Nanocrystal-Based Single Microdisk Resonator. *Opt. Express* **2008**, *16*, 13218–13224.
13. Kekatpure, R. D.; Brongersma, M. L. Fundamental Photophysics and Optical Loss Processes in Si-Nanocrystal-Doped Microdisk Resonators. *Phys. Rev. A* **2008**, *78*, 023829.
14. Song, Q.; Cao, H.; Ho, S. T.; Solomon, G. S. Near-IR Subwavelength Microdisk Lasers. *Appl. Phys. Lett.* **2009**, *94*, 061109.
15. Zhang, Z. Y.; Yang, L.; Liu, V.; Hong, T.; Vahala, K.; Scherer, A. Visible Submicron Microdisk Lasers. *Appl. Phys. Lett.* **2007**, *90*, 111119.
16. Fallert, J.; Stelzl, F.; Zhou, H.; Reiser, A.; Thonke, K.; Sauer, R.; Klingshirn, C.; Kalt, H. Lasing Dynamics in Single ZnO Nanorods. *Opt. Express* **2008**, *16*, 1125–1131.
17. Gargas, D. J.; Toimil-Molares, M. E.; Yang, P. D. Imaging Single ZnO Vertical Nanowire Laser Cavities Using UV-Laser Scanning Confocal Microscopy. *J. Am. Chem. Soc.* **2009**, *131*, 2125–2127.
18. Huang, M. H.; Mao, S.; Feick, H.; Yan, H. Q.; Wu, Y. Y.; Kind, H.; Weber, E.; Russo, R.; Yang, P. D. Room-Temperature Ultraviolet Nanowire Nanolasers. *Science* **2001**, *292*, 1897–1899.
19. Nobis, T.; Kaidashev, E. M.; Rahm, A.; Lorenz, M.; Grundmann, M. Whispering Gallery Modes in Nanosized Dielectric Resonators with Hexagonal Cross Section. *Phys. Rev. Lett.* **2004**, *93*, 103903.
20. Zimmler, M. A.; Bao, J.; Capasso, F.; Muller, S.; Ronning, C. Laser Action in Nanowires: Observation of the Transition from Amplified Spontaneous Emission to Laser Oscillation. *Appl. Phys. Lett.* **2008**, *93*, 051101.
21. Czekalla, C.; Sturm, C.; Schmidt-Grund, R.; Cao, B. Q.; Lorenz, M.; Grundmann, M. Whispering Gallery Mode Lasing in Zinc Oxide Microwires. *Appl. Phys. Lett.* **2008**, *92*, 241102.
22. Ursaki, V. V.; Burlacu, A.; Rusu, E. V.; Postolake, V.; Tiginyanu, I. M. Whispering Gallery Modes and Random Lasing in ZnO Microstructures. *J. Opt. A: Pure Appl. Opt.* **2009**, *11*, 075001.
23. Liu, J. Z.; Lee, S.; Ahn, Y. H.; Park, J. Y.; Koh, K. H.; Park, K. H. Identification of Dispersion-Dependent Hexagonal Cavity Modes of an Individual ZnO Nanonail. *Appl. Phys. Lett.* **2008**, *92*, 263102.
24. Wang, D.; Seo, H. W.; Tin, C. C.; Bozack, M. J.; Williams, J. R.; Park, M.; Tzeng, Y. Lasing in Whispering Gallery Mode in ZnO Nanonails. *J. Appl. Phys.* **2006**, *99*, 093112.
25. Yan, H. Q.; He, R. R.; Pham, J.; Yang, P. D. Morphogenesis of One-Dimensional ZnO Nano- and Microcrystals. *Adv. Mater.* **2003**, *15*, 402–405.
26. Slusher, R. E.; Levi, A. F. J.; Mohideen, U.; McCall, S. L.; Pearton, S. J.; Logan, R. A. Threshold Characteristics of Semiconductor Microdisk Lasers. *Appl. Phys. Lett.* **1993**, *63*, 1310–1312.
27. Ushigome, R.; Fujita, M.; Sakai, A.; Baba, T.; Kokubun, Y. Gainasp Microdisk Injection Laser with Benzocyclobutene Polymer Cladding and Its Athermal Effect. *Jpn. J. Appl. Phys.* **2002**, *41*, 6364–6369.
28. Taflove, A.; Hagness, S. C. *Computational Electrodynamics: The Finite-Difference Time-Domain Method*; Artech: Norwood, MA, 2000.
29. Farjadpour, A.; Roundy, D.; Rodriguez, A.; Ibanescu, M.; Bermel, P.; Joannopoulos, J. D.; Johnson, S. G.; Burr, G. W. Improving Accuracy by Subpixel Smoothing in the Finite-Difference Time Domain. *Opt. Lett.* **2006**, *31*, 2972–2974.
30. Chang, S. W.; Chuang, S. L. Fundamental Formulation for Plasmonic Nanolasers. *IEEE J. Quantum Electron.* **2009**, *45*, 1014–1023.